Published in final edited form as:
Curr Cardiovasc Imaging Rep. 2011 February 1; 4(1): 50–62. doi:10.1007/s12410-010-9055-3.

Cellular and Functional Imaging of Cardiac Transplant Rejection

Yijen L. Wu,
Pittsburgh NMR Center for Biomedical Research and the Department of Biological Sciences, Carnegie Mellon University, Pittsburgh, PA, USA

Qing Ye, and
Pittsburgh NMR Center for Biomedical Research and the Department of Biological Sciences, Carnegie Mellon University, Pittsburgh, PA, USA

Chien Ho
Pittsburgh NMR Center for Biomedical Research and the Department of Biological Sciences, Carnegie Mellon University, Pittsburgh, PA, USA; Department of Biological Sciences, Carnegie Mellon University, 4400 Fifth Avenue, Pittsburgh, PA 15213, USA

Chien Ho: chienho@andrew.cmu.edu

Abstract

Heart transplantation is now an established treatment for patients suffering from end-stage heart diseases. With the advances in immunosuppressive treatment, the survival rate for transplant patients has improved greatly. However, allograft rejection, both acute and chronic, after heart transplantation is still a limitation leading to morbidity and mortality. The current clinical gold standard for screening rejection is endomyocardial biopsy (EMB), which is not only invasive, but also error-prone, due to the limited sample size and the site location of sampling. It would be highly desirable to have reliable and noninvasive alternatives for EMB in monitoring cardiac allograft rejection. The objective of this review is to highlight how cardiovascular imaging can contribute to noninvasively detecting and to evaluating both acute and chronic allograft rejection after heart transplantation, in particular, cardiovascular MRI (CMRI); and how CMRI can assess both immune cell infiltration at the rejecting organ, and the cardiac dysfunctions resulting from allograft rejection.

Keywords

Cardiac MRI; Heart transplantation; Rejection; Macrophage; Lymphocyte; Cell tracking; Tagging; Iron oxide nanoparticles

Introduction

Since the first successful renal transplantation in 1954, and heart transplantation in 1967, solid organ transplantation has saved many lives of those suffering from end-stage organ failure. The survival rates and the quality of life for transplant patients have markedly improved during the last two decades due to the development of immunosuppressive drugs and advances in organ preservation and transplant technology. There is pivotal importance for appropriate immunosuppressive therapy, balancing between allograft rejection and immune deficiency. Recurrent rejection episodes leading to the accumulative tissue damage

Correspondence to: Chien Ho, chienho@andrew.cmu.edu.

Disclosure No potential conflicts of interest relevant to this article were reported.

can lead to massive myocardial necrosis and eventually graft loss. On the other hand, overdosing with immunosuppressive drugs can put patients in danger of potential pathological conditions due to immune deficiency and infection. Therefore, accurate and sensitive evaluation of the rejection status is crucial for proper management of cardiac grafts, determination of therapeutic strategy, and patient welfare.

Current standard practices for monitoring rejection after heart transplantation are relying on invasive procedures: endomyocardial biopsy (EMB) [1,2] for acute rejection surveillance; and coronary angiography or intravascular ultrasound (IVUS) for chronic rejection diagnosis [3]. These procedures need to be repeated over the life of the heart transplant patients. They are not only invasive and costly, but the accuracy is less than ideal (due to a limited number of myocardial zones that can be biopsied). Although widely used, EMB is invasive, associated with finite risks of morbidity and mortality, and is prone to sampling errors due to limited sample sizes and locations available, especially in pediatric patients. In addition, the interpretation of EMB can be subjective, resulting in erroneous diagnosis and inability to predict the onset of rejection. There is an urgent need for noninvasive and reliable alternatives.

Various imaging modalities, such as echocardiography, positron emission tomography (PET), CT, optical, and MRI, offer great potential for noninvasive detection of rejection. See Christen et al. [4] and Estep et al. [5] for comprehensive reviews for multimodality imaging for rejection; Butler et al. [6] for a detailed summary for early MRI for rejection; and Mondillo et al. [7] for echocardiography. In recent years, peripheral biomarkers and gene expression profiles [8] are emerging as potentially promising indicators for monitoring rejection. In addition, multimodality molecular imaging [9•] has widened the horizon for rejection investigation. The scope of this review focuses on highlighting the current advancement of cellular and functional cardiovascular MRI (CMRI) for noninvasive evaluation of allograft cardiac rejection after heart transplantation, in both the preclinical animal models and clinical arena.

Cardiac Allograft Rejection

Allograft rejection (AR) occurs when the recipient immune system recognizes the transplanted organ as a foreign object and triggers a cascade of molecular and cellular immune responses. Acute cellular rejection (ACR) occurs days to months, sometimes years, after organ transplantation due to mismatched histocompatibility between donor organ and the recipient. The hallmark of acute rejection is the lymphocytic and monocytic infiltration, followed by endothelial cellular injury and structural tissue deterioration and myocardial necrosis [1,2]. Despite the advancement of immunosuppressants, acute rejection episodes still occur in 40% to 70% of heart transplants during the first 6 months [10]. Cardiac transplant patients on average have one to three episodes of AR within the first year after transplantation [11]. When AR occurs, responding to donor antigens, immune cells, including macrophages, T cells, and other host immune cells, infiltrate the graft. Activation and infiltration of immune cells at the rejecting graft gives rise to inflammation, increased myocytolysis, myocardial edema, and myocyte necrosis. ACR is found in most AR cases, but antibody-mediated humoral rejection, which accounts for most of the biopsy-negative episodes of rejection [12], is associated with accelerated graft coronary artery diseases, increased graft loss, and increased mortality. Recurrent episodes of acute rejection and severity are strongly associated with the later development of chronic rejection [13,14].

Chronic rejection, or chronic allograft vasculopathy (CAV), manifests years after transplantation, and is the main cause of long-term (5 years and beyond) graft loss and mortality. The hallmark of the chronic rejection is the interstitial fibrosis and proliferative

vasculopathy affecting all intra-graft arteries [15,16]. CAV is a unique form of atherosclerosis, caused by combination of immunological factors and non-immunological players. Different from classic atherosclerosis with focal and eccentric luminal narrowing, CAV displays distal-to-proximal progression of diffused concentric vascular narrowing, from small vessels to larger ones. The chronic inflammatory and immune response against the transplanted graft is not well understood, the progression of the CAV is still unpredictable, and the correct detection is still challenging [5]. An accurate means of diagnosis of chronic rejection is a pressing need in treating organ rejection.

Rodent and Murine Models for Cardiac Allograft Rejection Research

Heterotopic heart and lung transplantation models in rats and mice [17–20] have been instrumental in cardiac rejection research. In the heterotopic transplantation models, the recipient animal receives an additional heart or heart-lung other than in the chest, and the native heart supports the host survival, so that the entire process of the rejection can be studied with only minimally possible perturbation of host hemo-physiology systemically. The end-to-side anastomosis of the graft vessels to recipient vessels results in fully vascularized graft. Many variations of the vascular configurations and graft locations (abdominal, inguinal, or cervical) have served different purposes of investigation. The non-working heart model is technologically easier and might be suitable for immunological and cellular investigation, but not feasible for functional investigation due to insufficient left ventricular workload [21•]. On the other hand, a working heart model is technologically more challenging, but is more adequate for functional investigation, and allows closer-to-native myocardial perfusion and cellular infiltration [22•,23,24,25•,26•].

There are arrays of inbred strains of rats and mice available for transplantation studies. Across-strain transplantation, the allograft transplantation will result in allograft rejection, whereas transplantation within the same strain, the isograft or “self” transplantation, like transplantation between identical twins, produces no rejection, and serves as an isogeneic control. Different strain combinations for transplantation produce different degrees of allograft rejection, thus permitting different degrees of approximation to clinical conditions. Although technically more challenging due to small size, mice provide more genetically manipulated transgenic or knockout strains, which makes selective molecular investigation of rejection mechanisms possible. On the other hand, rats are much easier to operate on, and allow more sensitive and sophisticated imaging schemes.

Treating the allograft transplantation with different regimens of immunosuppressant drugs mimics the clinical settings of rejection. With sufficient suppression of acute rejection, grafts are allowed to develop chronic rejection over time. It is always difficult to differentiate the primary or secondary effects of immunosuppressant drugs in respect to rejection in the clinical arena, because immunosuppressant drugs are necessary for human transplantation patients [10,27]. Recently, the development of a single major histocompatibility complex gene–mismatched rat strain permitted allograft transplantation with almost no acute rejection [28]. Transplantation from PVG.1U (RT1.A^uB^u-D^uC^u) to PVG.R8 (RT1.$A^aB^uD^uC^u$) rats exhibits almost no acute rejection, and allografts develop chronic rejection in the absence of acute rejection and immunosuppressive manipulation, most evidently after 100 days. A distinct advantage of this single gene–mismatched rodent model is the antigenic simplicity without immunomodulation. This genetic model enables investigation that cannot be achieved in clinical conditions, thus facilitating studies aimed at the elucidation of immunological mechanisms of chronic allograft rejection, including the effects of immunosuppressive drugs.

Cardiovascular Imaging for Detecting Cardiac Allograft Rejection

Detection of Rejection with CMRI in the Clinical Arena

Up to now, most of the clinical applications for detecting cardiac allograft rejection with CMRI are mainly detecting manifestation of the rejection in the tissue or organ levels, viewing allograft rejection as one of the pathological states of the heart [4,6–8]. Reduced ejection fraction (EF) [5,6,29], prolonged T_2 [5,6,30], altered T_1, hyperenhancement with delayed enhancement (DE), and elevated Gd-based contrast agent uptake [5,6,31] have been found to be associated with cardiac allograft rejection, probably due to edema, necrosis, and fibrosis resulting from rejection. Decreased myocardial perfusion [5,6,32,33] and changes in myocardial perfusion reserve have been found in transplant patients suffering from CAV. Combinations of multiparameter CMRI, accessing cine, T_1/T_2, perfusion, and DE together, can make a good diagnosis of compromised heart conditions with rejection in one CMRI session [34–36]. In addition, ^{31}P MR chemical shift imaging [37] has also been found to change in a small cohort of CAV patients.

Although powerful, current CMRI is more useful for confirming rejection diagnosis with noticeable clinical symptoms, or tracking progress of cardiac function improvement upon treatments, because current CMRI is detecting later expression in the rejection cascade, such as edema, necrosis, and fibrosis, when the myocardial injury has already occurred. However, the majority of patients with earlier ACR show no significant changes in EF or standard global systolic functions [5,6]. In addition, patients with CAV are usually without angina due to denervation of the graft heart, so they are unaware of CAV development. By the time the clinical symptoms are presented, or depressed global systolic cardiac functions are detected, it is often beyond the point for effective therapy to fully restore the graft health. In addition, many of the CMRI indicators for ill-functioned heart are shared with other pathological conditions of the heart; hence specific diagnosis of rejection with CMRI alone is difficult.

Our goal is to develop more sensitive CMRI methodology that is able to detect earlier or milder phases of allograft rejection, before irreversible tissue damage occurs (ie, before clinical symptoms emerge), to allow opportunities for clinical intervention and therapy. We have employed a two-pronged approach with cellular and functional MRI, to monitor both the immune cell infiltration at the rejecting heart, as well as the earlier local cardiac dysfunction and strain abnormality resulting from rejection, in search for sensitive and reliable noninvasive CMRI parameters for correct diagnosing of rejection in early milder rejection phases before irreversible tissue damage occurs.

Cellular CMRI for Rejection

T-lymphocytes are thought to coordinate both acute and chronic rejection. Macrophages are present in large quantity throughout the entire rejection process. B-lymphocytes, dendritic cells (DCs), as well as endothelial cells all play a role in the rejection process. The presence of these various immune cell types can indicate the status of rejection. Detecting and profiling the temporal and spatial relationships of these cells with CMRI can serve as potential surrogate markers for rejection.

To make the cells of interest detectable with MRI, a substantial differentiation in signal needs to be created between the target cells and the surrounding tissues. This can be achieved by labeling the target cells, such as macrophages and T-lymphocytes, with MR contrast agents. Iron oxide (Fe_nO_m) particles have been the most commonly used MR contrast agent for cell tracking, because of their ability to cause large ^{1}H signal perturbation, resulting in considerable hypointensity in T_2*-weighted MR images.

Iron oxide nanoparticles are composed of Fe_2O_3 and Fe_3O_4 cores, and are usually stabilized by different coating materials, which shield the metallic core and make the particles biocompatible. Coating materials, such as dextran, polyethylene glycol (PEG), or other polysaccharide derivatives, are bio-degradable; some materials, such as styrene-divinyl benzene inert polymers, are not biodegradable. The overall hydrodynamic sizes of the particles and the coating materials not only determine the in vivo lifetime of the particles in the labeled cells and in the blood stream, but also the extent of incorporation of the particles into the cells. Superparamagnetic iron oxide (SPIO) and ultra-small superparamagnetic iron oxide (USPIO) nanoparticles consist of compatible iron core sizes (4–5 nm and 5–8 nm, respectively) and similar surface coating materials, yet different total hydrodynamic sizes (120–180 nm and 15–30 nm). On the other hand, the much larger micrometer-sized particles, MPIO, usually composed of a magnetite core and an inert coat, are around 1 μm to several micrometers. Because of the large core magnetite contents, one single MPIO particle contains more than 1 pg of iron, whereas it takes a few more degrees of magnitudes of SPIO or USPIO particles to achieve the same amount.

The MR labels can be introduced into the target cells via one of two main routes. In the ex vivo or in vitro labeling schemes, the cells of interest isolated from the host or cell lines are tagged with MR markers in culture, and the labeled cells are then introduced into the subject. In the in vivo or in situ labeling schemes, MR labeling agents are administered systemically and the target cells phagocytose MR labels in their natural biological environments without cell isolation or culture.

Cellular Imaging of Macrophages in Acute Rejection

Macrophages, being phagocytotic, can be easily labeled in vivo, or in situ. MR contrast agents present in the circulation can be ingested by circulating monocytes/macrophages, which migrate to the rejection sites [21•,22•,23,24,25•,26•,38–40]. One day after in vivo USPIO labeling (Fig. 1), patches of hypointensity can be seen through the left ventricle (LV) and right ventricle (RV) of allograft hearts [22•]. Dark areas are concentrated foci of iron-laden macrophages, which are confirmed by pathological ED1 staining of macrophages. Macrophage-infiltrated foci appear to be highly heterogeneous in space. Thus, sampling errors are likely to result when probing rejection with biopsy needles. EMB samples are usually taken from anteroseptal wall of the RV, which does not appear to have high concentration of macrophage infiltration. It is not surprising, then, to find EMB sampling that does not reflect the actual cellular infiltration status of the graft. Monitoring rejection with cellular CMRI is not only noninvasive, but also provides a valuable overall three-dimensional whole-volume perspective of rejection.

USPIO and SPIO nanoparticles with dextran coating are biocompatible and biodegradable. The externally administered nanoparticles can be digested and incorporated into the systemic iron pool over time. Thus, the hypointensity can be “reversible” depending on the observation time window. Repetitive imaging over a longer time period requires repetitive administration of the nanoparticles prior to imaging. It has been found that the hypointensity reflects rejection status of the grafts. In both cardiac [21•,22•,23,24,25•,26•] and renal transplants [41,42], the degree of hypointensity increases as the rejection progresses, decreases upon cyclosporine immunosuppressive treatment, and the extent of hypointensity increases again after withdrawing the immunosuppressive drug [21•]. The biodegradable SPIO and USPIO are found to be tolerated well, incorporating into body iron pool upon metabolism [43], and imposing very little safety and toxicity concerns [44]. A similar type of particles, Feridex, is approved by the US Food and Drug Administration for human use. The clinical translation for cellular imaging with MRI is feasible.

MPIO, the larger micrometer-sized iron-oxide particles, due to its high iron content and special iron core structure that generates large background gradient and local magnetic field perturbation, makes imaging single or few cells in vivo possible [25•,45–47]. Various types of iron-oxide particles can give different but compatible contrast patterns in rejecting hearts [25•]. With in vivo labeling of MPIO particles, macrophage infiltration foci show punctate and circular dots (Fig. 2) at the location comparable to that with USPIO labeling. At earlier rejection phase, macrophage infiltration is more toward epicardium; as the rejection progresses over time, macrophage infiltration penetrates deeper into myocardium tissue. This cellular infiltration progression pattern is confirmed by pathology (Fig. 3) and it has not yet been observed by biopsy due to limited sizes of the biopsy tissues. MRI is not only noninvasive, but also can provide an entire whole-volume perspective of the rejection processes over time.

MPIO, with current styrene-divinyl benzene inert polymer coating, are not biodegradable. Although having extremely short blood half-life (minutes), the labels are stable for long periods of time (many months) once ingested into cells, allowing repetitive observation without further administration. After single injection of MPIO particles, only little hypointensity was observed in early days while no or little rejection occurs. As rejection progresses over time, even without further administration of particles, greater areas of more hypointensity are seen while more MPIO-labeled macrophages are recruited into the rejecting graft heart [25•]. Thus, single MPIO administration permits repetitive longitudinal monitoring of the entire rejection process.

Cellular Imaging of Macrophages in Chronic Rejection

With detailed cellular and molecular mechanisms that still need to be elucidated, CAV remains the major challenge for heart transplantation. MPIO particles, with stable and inert polymer coating and large quantity of iron contents, are suitable for long-term tracking of immune cells in CAV. Single administration of MPIO particles allows longitudinal observation of the same subject over a long period of time for a few months, allowing repetitive imaging of chronic rejection [26•].

In our single-gene mismatch PVG transplantation model, CAV develops over a few months of time, with no need for immunosuppressive treatments. It is found that macrophages appear very early in the CAV [26•], and increase as CAV progresses to be more evident (Figs. 4 and 5). Macrophages can be an early marker for CAV [26•], prior to presentation of clinical symptoms, offering sensitive early detection of CAV.

Many iron oxide particles are also designed to contain fluorescent tags (Fig. 6). Multimodality cell tracking probes allow for both MR and optical imaging [9•,22•,25•,26•, 45–48]. In addition, MR probes with different colors of fluorescent tags can facilitate molecular and cellular mechanistic investigation for rejection biology.

Imaging Other Immune Cell Types in Rejection

Non-phagocytotic cells, such as T-lymphocytes, B-lymphocytes, or bone marrow–derived mesenchymal stem cells (MSCs), unlike phagocytotic macrophages, cannot readily take up MRI contrast agents. They cannot be labeled efficiently in vivo or in situ, but need to be labeled ex vivo in culture. The labeling efficiency for T-lymphocytes with currently available iron oxide nanoparticles is low (around 10% to 25%) with simple co-incubation in culture. Some external manipulation is usually necessary to label T cells with sufficient amounts of iron (at least 1 pg per cell), such as electroporation, positively charged transfection agents, attaching to HIV-tat peptide, or receptor-mediated endocytosis [23].

We have been developing a new class of iron oxide particles [48] that can be more readily ingested by the non-phagocytotic cell types, for efficient labeling for cellular MRI. The newly synthesized, PEG-coated, nano-sized iron oxide particle, ITRI-IOP (Fig. 7), can label phagocytic macrophages and DCs, as well as non-phagocytic bone marrow–derived MSCs isolated from rats in vitro with ITRI-IOP without the use of additional agents or manipulation (Fig. 8). The labeling efficiency is as high as 92% to 99%, and the labeled cells show larger T_2* perturbation compared to commercially available USPIO and SPIO particles. In addition, ITRI-IOPs yield comparable hypointensity and imaging quality with MPIO particles when labeling macrophages in vivo. We have been able to label T cells with high efficiency without aiding agents using these particles (unpublished results). ITRI-IOPs and their different classes of derivatives are promising reagents for efficient non-phagocytotic cell labeling for imaging allograft rejection and other cell tracking research.

One potential limitation of macrophage imaging is that it is difficult to distinguish early ischemic injury and inflammation from rejection [4]. Using different tags to label T cells and macrophages will allow us to further discern correct cellular profiles throughout the rejection process.

Functional CMRI for Rejection

Global systolic functions and other current CMRI parameters appear to be normal with no significant alternation until the later stage of rejection, when myocardial injury has already taken place. To detect potential early mild local changes in cardiac function without significant changes in global systolic functions, tagging CMRI (Fig. 9) is implemented to look for early local changes in wall motion and strains in mild rejection. Tagging CMRI places signal-void grids on tissue by saturating proton spins at designated planes in space prior to the imaging sequence and these grids serve as the material points for tracking heart motion, to mark tissue elongation, stretching, or depression and shortening. Strain analysis can quantify regional ventricular wall motion and tissue deformation in high precision.

Our recent results [22•] have shown that early changes in ventricular wall motion, like immune cell infiltration, are heterogeneous (Fig. 1). The early changes of regional strains also appear to be highly heterogeneous (Figs. 9 and 10). Early mild subtle changes in local strain and ventricular wall motion can be detected while no significant changes in EF and stroke volume are observed. The degrees of local strain changes correlate well with rejection status, even when no changes are found in global systemic functions (Fig. 11). Since cellular infiltration causing local contractile abnormality is not necessarily following the coronary territories, and can happen in any locations of the heart, tagging MRI with high-resolution strain analysis can permit analysis of regional wall motion with high resolution, free from coronary architecture, and is not limited to the conventional 17-segment model (Fig. 10). While overall strain analysis and modeling can be labor intensive, clinically relevant indexes can be extracted (Fig. 12) for potential clinical translation.

Our findings in regional strain abnormality without alternation in global systolic functions (EF) in early rejection are consistent with recent development of detecting strain and strain rate changes in rejection with echocardiography [49,50].

There is encouraging addition of accuracy in diagnosing rejection when simultaneously assessing both cellular imaging of macrophage infiltration and regional functional strain analysis (Fig. 10). While there are fine individual variations of the degrees of cellular infiltration and of local strain abnormality, individuals with more immune cell infiltration show greater degrees of compromised strains (Fig. 13), reflecting finer degrees of deterioration. Simultaneous coupling of cellular and functional aspects of rejection adds further accuracy and sensitivity for detecting rejection. Our two-pronged approach with

cellular and functional MRI for both cellular infiltration and strains provides a promising potential for noninvasive rejection detection. More detailed analysis with larger sample sizes might lead to possible finer staging of rejection within the current mild to moderate rejection grades (I, IIA, and IIB) defined by EMB, and can offer a more precise and sensitive method for assessing ACR.

Conclusions

Our two-pronged approach with simultaneous cellular and functional MRI provides potential noninvasive and early detection of rejection before irreversible tissue damage has taken place. In vivo cellular MRI for macrophages and lymphocytes provides whole-volume perspective of graft rejection. With the development of more novel contrast agents, one can tailor the cellular MRI for complex cellular and molecular mechanistic investigation for ACR and CAV. Detailed profiling and modeling of the temporal and spatial relationship of the overall rejection cascade involving various cell types can establish surrogate markers for various stages of rejection. In vivo functional MRI together with high-resolution tagging MRI and strain analysis not only offers great potential to look beyond the mere cell location or temporal-spatial distribution of cells, but also provides multimodal information for functions and compositions. Together, cellular and functional CMRI formulation can be established for finer and more sensitive rejection grading noninvasively. In combination with current CMRI, capable of noninvasively assessing myocardial injury, it is conceivable to build an integrated multiparameter CMRI “tool kit,” covering many different aspects of allograft rejection, for more comprehensive diagnosis of cardiac allograft rejection.

Acknowledgments

This work is supported by National Institutes of Health grants (R01HL-081349 and P41EB-001977).

References

Papers of particular interest, published recently, have been highlighted as:

• Of importance

1. Nair V, Butany J. Heart transplant biopsies: interpretation and significance. J Clin Pathol 2010;63:12–20. [PubMed: 19858528]
2. Stewart S, Winters GL, Fishbein MC, et al. Revision of the 1990 working formulation for the standardization of nomenclature in the diagnosis of heart rejection. J Heart Lung Transplant 2005;24:1710–1720. [PubMed: 16297770]
3. Mehra MR, Crespo-Leiro MG, Dipchand A, et al. International Society for Heart and Lung Transplantation working formulation of a standardized nomenclature for cardiac allograft vasculopathy–2010. J Heart Lung Transplant 2010;29:717–727. [PubMed: 20620917]
4. Christen T, Shimizu K, Libby P. Advances in imaging of cardiac allograft rejection. Curr Cardiovasc Imaging Rep 2010;3:99–105.
5. Estep JD, Shah DJ, Nagueh SF, et al. The role of multimodality cardiac imaging in the transplanted heart. JACC Cardiovasc Imaging 2009;2:1126–1140. [PubMed: 19761994]
6. Butler CR, Thompson R, Haykowsky M, et al. Cardiovascular magnetic resonance in the diagnosis of acute heart transplant rejection: a review. J Cardiovasc Magn Reson 2009;11:7. [PubMed: 19284612]
7. Mondillo S, Maccherini M, Galderisi M. Usefulness and limitations of transthoracic echocardiography in heart transplantation recipients. Cardiovasc Ultrasound 2008;6:2. [PubMed: 18190712]
8. Mehra MR, Uber PA, Benitez RM. Gene-based bio-signature patterns and cardiac allograft rejection. Heart Fail Clin 2010;6:87–92. [PubMed: 19945064]

9•. Christen T, Nahrendorf M, Wildgruber M, et al. Molecular imaging of innate immune cell function in transplant rejection. Circulation 2009;119:1925–1932. [PubMed: 19332470] The authors took a step further to investigate which macrophage functions are important in allograft rejection by probing the innate immunity with quenched fluorescent substrate reporter for cathepsin proteases and a nanoparticle-based phagocytosis sensor, along with cellular MRI tracking macrophages in vivo in a mouse model.

10. Lindenfeld J, Miller GG, Shakar SF, et al. Drug therapy in the heart transplant recipient: part II: immunosuppressive drugs. Circulation 2004;110:3858–3865. [PubMed: 15611389]

11. Gradek WQ, D'Amico C, Smith AL, et al. Routine surveillance endomyocardial biopsy continues to detect significant rejection late after heart transplantation. J Heart Lung Transplant 2001;20:497–502. [PubMed: 11343975]

12. Fishbein MC, Kobashigawa J. Biopsy-negative cardiac transplant rejection: etiology, diagnosis, and therapy. Curr Opin Cardiol 2004;19:166–169. [PubMed: 15075746]

13. Jimenez J, Kapadia SR, Yamani MH, et al. Cellular rejection and rate of progression of transplant vasculopathy: a 3-year serial intravascular ultrasound study. J Heart Lung Transplant 2001;20:393–398. [PubMed: 11295576]

14. Yamani MH, Yousufuddin M, Starling RC, et al. Does acute cellular rejection correlate with cardiac allograft vasculopathy? J Heart Lung Transplant 2004;23:272–276. [PubMed: 15019635]

15. Mitchell RN. Graft vascular disease: immune response meets the vessel wall. Annu Rev Pathol 2009;4:19–47. [PubMed: 18717641]

16. Suzuki J, Isobe M, Morishita R, Nagai R. Characteristics of chronic rejection in heart transplantation: important elements of pathogenesis and future treatments. Circ J 2010;74:233–239. [PubMed: 20009354]

17. Martins PN. Assessment of graft function in rodent models of heart transplantation. Microsurgery 2008;28:565–570. [PubMed: 18767132]

18. Steinbruchel DA, Nielsen B, Salomon S, Kemp E. A new model for heterotopic heart transplantation in rodents: graft atrial septectomy. Transplant Proc 1994;26:1298–1299. [PubMed: 8029913]

19. Asfour B, Hare JM, Kohl T, et al. A simple new model of physiologically working heterotopic rat heart transplantation provides hemodynamic performance equivalent to that of an orthotopic heart. J Heart Lung Transplant 1999;18:927–936. [PubMed: 10561102]

20. Hasegawa T, Visovatti SH, Hyman MC, et al. Heterotopic vascularized murine cardiac transplantation to study graft arteriopathy. Nat Protoc 2007;2:471–480. [PubMed: 17406609]

21•. Kanno S, Wu YJ, Lee PC, et al. Macrophage accumulation associated with rat cardiac allograft rejection detected by magnetic resonance imaging with ultrasmall superparamagnetic iron oxide particles. Circulation 2001;104:934–938. [PubMed: 11514382] This is the first successful demonstration of in vivo detection of macrophage accumulation in the rejecting allograft hearts with MRI and its relationship with immunosuppressive agents in a rodent non-working heart model.

22•. Wu YL, Ye Q, Sato K, et al. Noninvasive evaluation of cardiac allograft rejection by cellular and functional cardiac magnetic resonance. JACC Cardiovasc Imaging 2009;2:731–741. [PubMed: 19520344] The authors used a two-pronged cellular and functional MRI approach to evaluate cardiac rejection in a rodent working heart transplant model by simultaneously monitoring both the macrophage accumulation in the rejecting hearts and local ventricular wall motion with fine strain analysis The results show that the early mild allograft rejection is very heterogeneous and that the multiparameter CMRI has the potential to provide accurate noninvasive diagnosis of cardiac rejection.

23. Ho C, Hitchens TK. A non-invasive approach to detecting organ rejection by MRI: Monitoring the accumulation of immune cell cells at the transplanted organ. Curr Pharmaceut Biotechnol 2004;5:551–566.

24. Wu YJL, Sato K, Qing Y, Ho C. MRI investigation of graft rejection following organ transplantation using rodent models. Method Enzymol 2004;386:73–105.

25•. Wu YL, Ye Q, Foley LM, et al. In situ labeling of immune cells with iron oxide particles: an approach to detect organ rejection by cellular MRI. Proc Natl Acad Sci U S A 2006;103:1852–

1857. [PubMed: 16443687] Using the micrometer-sized MPIO and the USPIO particles to monitor macrophage infiltration in a rodent working heart transplantation model, the results show temporal progression of macrophage infiltration in vivo.

26•. Ye Q, Wu YL, Foley LM, et al. Longitudinal tracking of recipient macrophages in a rat chronic cardiac allograft rejection model with noninvasive magnetic resonance imaging using micrometer-sized paramagnetic iron oxide particles. Circulation 2008;118:149–156. [PubMed: 18591438] This article reports a longitudinal monitoring of macrophage accumulation for more than 3 months in a single gene–mismatched chronic cardiac rejection transplantation model The results show that macrophages labeled with MPIO can serve as an early marker for CAV.

27. Kobashigawa JA, Patel JK. Immunosuppression for heart transplantation: where are we now? Nat Clin Pract Cardiovasc Med 2006;3:203–212. [PubMed: 16568129]

28. Shirwan H, Wu GD, Barwari L, et al. Induction of allograft nonresponsiveness after intrathymic inoculation with donor class I allopeptides. II. Evidence for persistent chronic rejection despite high levels of donor microchimerism. Transplantation 1997;64:1671–1676. [PubMed: 9422400]

29. Bellenger NG, Marcus NJ, Davies C, et al. Left ventricular function and mass after orthotopic heart transplantation: a comparison of cardiovascular magnetic resonance with echocardiography. J Heart Lung Transplant 2000;19:444–452. [PubMed: 10808151]

30. Marie PY, Angioi M, Carteaux JP, et al. Detection and prediction of acute heart transplant rejection with the myocardial T2 determination provided by a black-blood magnetic resonance imaging sequence. J Am Coll Cardiol 2001;37:825–831. [PubMed: 11693758]

31. Almenar L, Igual B, Martinez-Dolz L, et al. Utility of cardiac magnetic resonance imaging for the diagnosis of heart transplant rejection. Transplant Proc 2003;35:1962–1964. [PubMed: 12962864]

32. Muehling OM, Wilke NM, Panse P, et al. Reduced myocardial perfusion reserve and transmural perfusion gradient in heart transplant arteriopathy assessed by magnetic resonance imaging. J Am Coll Cardiol 2003;42:1054–1060. [PubMed: 13678930]

33. Rivard AL, Swingen CM, Blake D, et al. A comparison of myocardial perfusion and rejection in cardiac transplant patients. Int J Cardiovasc Imaging 2007;23:575–582. [PubMed: 17206459]

34. Taylor AJ, Vaddadi G, Pfluger H, et al. Diagnostic performance of multisequential cardiac magnetic resonance imaging in acute cardiac allograft rejection. Eur J Heart Fail 2010;12:45–51. [PubMed: 20023044]

35. Kim YJ, Kang SM, Hur J, et al. Images in cardiovascular medicine. Chronic cardiac transplant rejection: evaluation with magnetic resonance imaging. Circulation 2008;118:885–886. [PubMed: 18711025]

36. Usta E, Burgstahler C, Aebert H, et al. The challenge to detect heart transplant rejection and transplant vasculopathy noninvasively--a pilot study. J Cardiothorac Surg 2009;4:43. [PubMed: 19682394]

37. Caus T, Kober F, Marin P, et al. Non-invasive diagnostic of cardiac allograft vasculopathy by 31P magnetic resonance chemical shift imaging. Eur J Cardiothorac Surg 2006;29:45–49. [PubMed: 16343922]

38. Johansson L, Johnsson C, Penno E, et al. Acute cardiac transplant rejection: detection and grading with MR imaging with a blood pool contrast agent–experimental study in the rat. Radiology 2002;225:97–103. [PubMed: 12354991]

39. Penno E, Johnsson C, Johansson L, Ahlstrom H. Macrophage uptake of ultra-small iron oxide particles for magnetic resonance imaging in experimental acute cardiac transplant rejection. Acta Radiol 2006;47:264–271. [PubMed: 16613307]

40. Beckmann N, Cannet C, Zurbruegg S, et al. Macrophage infiltration detected at MR imaging in rat kidney allografts: early marker of chronic rejection? Radiology 2006;240:717–724. [PubMed: 16837667]

41. Ye Q, Yang D, Williams M, et al. In vivo detection of acute rat renal allograft rejection by MRI with USPIO particles. Kidney Int 2002;61:1124–1135. [PubMed: 11849467]

42. Yang D, Ye Q, Williams M, et al. USPIO-enhanced dynamic MRI: evaluation of normal and transplanted rat kidneys. Magn Reson Med 2001;46:1152–1163. [PubMed: 11746582]

43. Arbab AS, Yocum GT, Kalish H, et al. Efficient magnetic cell labeling with protamine sulfate complexed to ferumoxides for cellular MRI. Blood 2004;104:1217–1223. [PubMed: 15100158]

44. Bernd H, De Kerviler E, Gaillard S, Bonnemain B. Safety and tolerability of ultrasmall superparamagnetic iron oxide contrast agent: comprehensive analysis of a clinical development program. Invest Radiol 2009;44:336–342. [PubMed: 19661843]
45. Williams JB, Ye Q, Hitchens TK, et al. MRI detection of macrophages labeled using micrometer-sized iron oxide particles. J Magn Reson Imaging 2007;25:1210–1218. [PubMed: 17520727]
46. Shapiro EM, Skrtic S, Koretsky AP. Sizing it up: cellular MRI using micron-sized iron oxide particles. Magn Reson Med 2005;53:329–338. [PubMed: 15678543]
47. Shapiro EM, Sharer K, Skrtic S, Koretsky AP. In vivo detection of single cells by MRI. Magn Reson Med 2006;55:242–249. [PubMed: 16416426]
48. Chen C, Zhang H, Ye Q, et al. A new nano-sized iron-oxide particle with high sensitivity for cellular magnetic resonance imaging. Mol Imaging Biol. 2010 In press.
49. Dandel M, Hetzer R. Echocardiographic strain and strain rate imaging–clinical applications. Int J Cardiol 2009;132:11–24. [PubMed: 18760848]
50. Kato TS, Oda N, Hashimura K, et al. Strain rate imaging would predict sub-clinical acute rejection in heart transplant recipients. Eur J Cardiothorac Surg 2010;37:1104–1110. [PubMed: 20031437]

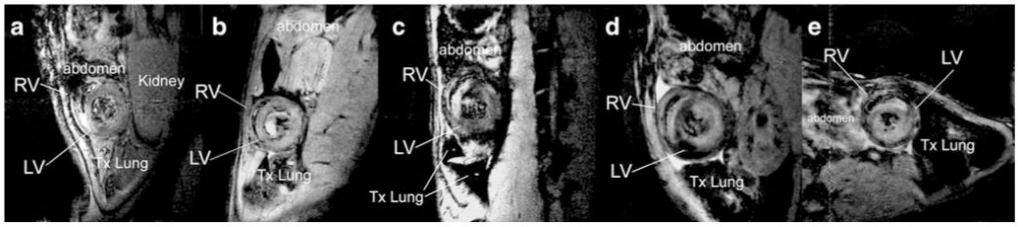

Fig. 1.

T_2*-weighted image showing USPIO-labeled immune cell infiltration in transplanted hearts. **a**, **b**, Isografts; **c**, **d**, Grade III allografts; and **e**, Grade II allograft. Patches of hypointensity indicate areas with high numbers of USPIO-labeled immune cells. The *upper left corner* of the isograft in *Panel a* has susceptibility artifact from the abdomen. LV—left ventricle; RV—right ventricle. (From Wu et al. [22•]; with permission)

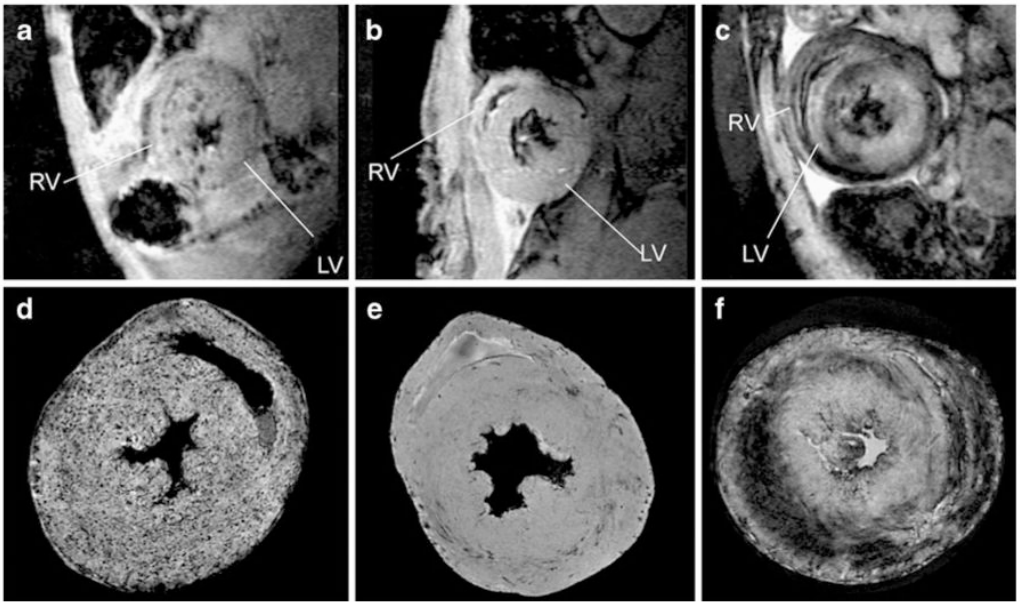

Fig. 2.

Contrast patterns with different contrast agent labeling. **a**–**c**, In vivo MRI of macrophage accumulation on POD 6 of **a** an allograft heart with MPIO-particle labeling; **b** an isograft heart with MPIO-particle labeling; and **c** an allograft heart with USPIO labeling, with 156 μm in-plane resolution at 4.7-Tesla **d**–**f**. MRM at 11.7-Tesla Bruker AVANCE-DBX MRI instrument with in-plane resolution of 40 μm of **d** an allograft heart with MPIO-particle labeling; **e** an isograft heart; and **f** an allograft heart with USPIO labeling. LV—left ventricle; RV—right ventricle. (From Wu et al. [25•]; with permission)

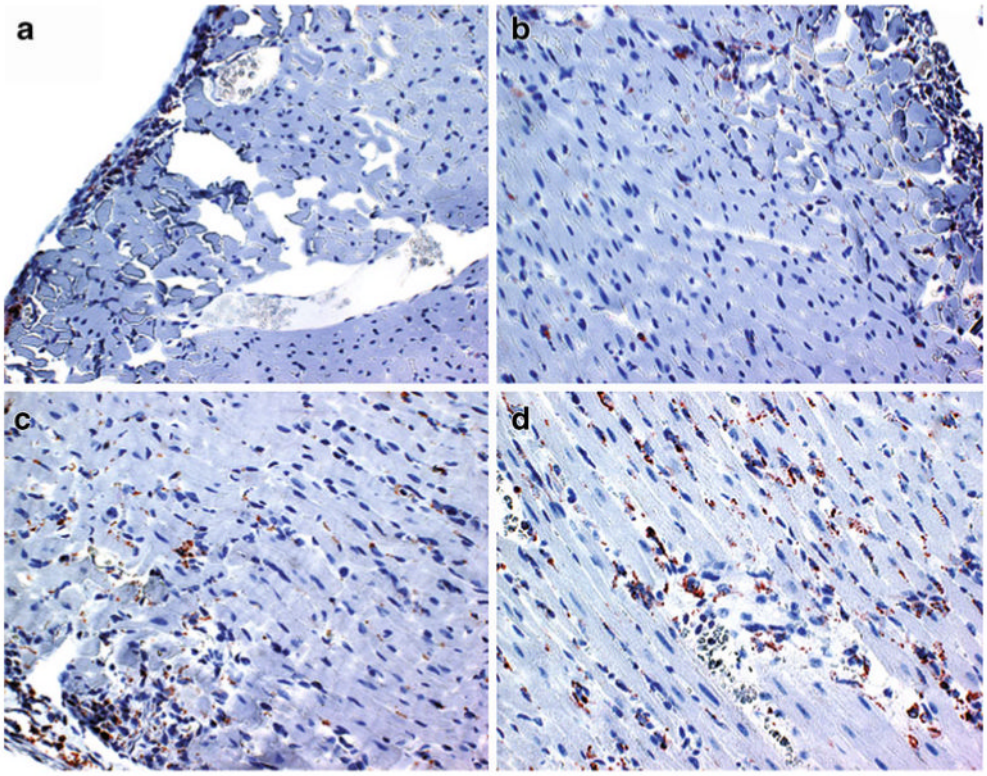

Fig. 3.

Temporal progression of ED1$^+$ macrophage infiltration. Optical micrograph (400× magnification) of anti-rat ED1$^+$ immunohistochemical staining sections of allograft hearts obtained on POD 3 **a**, POD 4 **b**, POD 5 **c**, and POD 6 **d**. The ED1$^+$ cells appear to be *brown* and the background is counter-stained *blue*. (From Wu et al. [25•]; with permission)

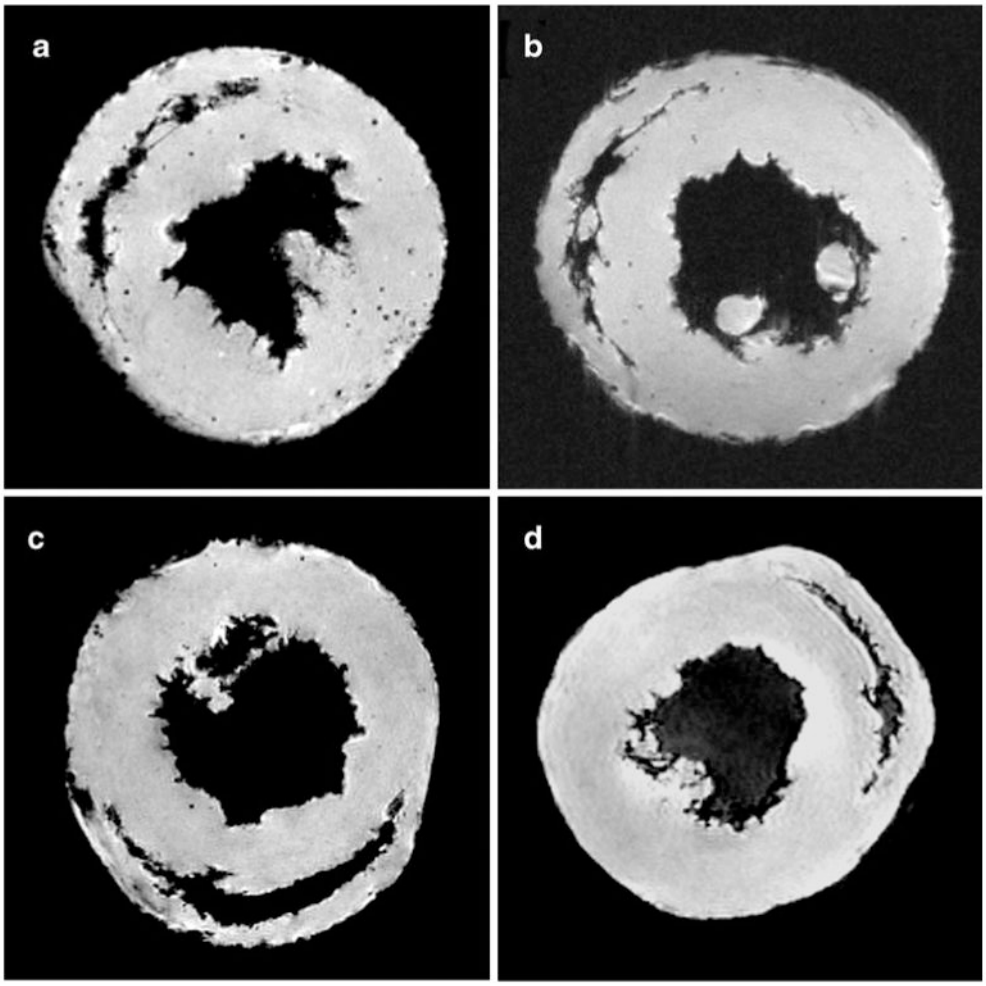

Fig. 4.

Representative MRM images of transplant and native hearts. Punctate regions of hypointensity can be clearly seen in the allograft heart harvested on POD 109 **a** after in vivo labeling with MPIO. A representative isograft heart harvested on POD 119 is shown in *Panel* **b**. Two native hearts are also shown **c** and **d**, one of which was harvested 7 days following MPIO injection **c**. (From Ye et al. [26•]; with permission)

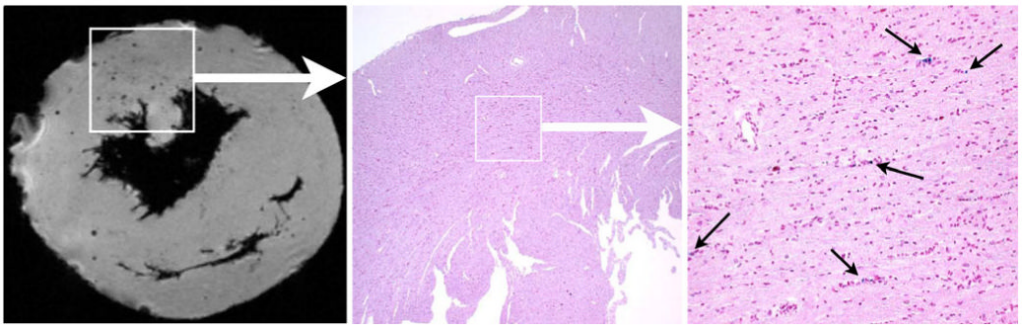

Fig. 5.

Correlation of MRM and iron staining of MPIO in a POD 94 allograft heart. Image from MRM shows the discrete and circular spots of hypointensity (*left panel*). These *black spots* of hypointensity effects are due to the presence of MPIO particles, which was confirmed by the matching section, that correspond to the same area as the *boxed region* in the MRM image on the *left*, stained with Perl's Prussian blue for iron (*center*, ×40 magnification). *Right image* shows the expansion of the *boxed region* in *center image* (×200 magnification). (From Ye et al. [26•]; with permission)

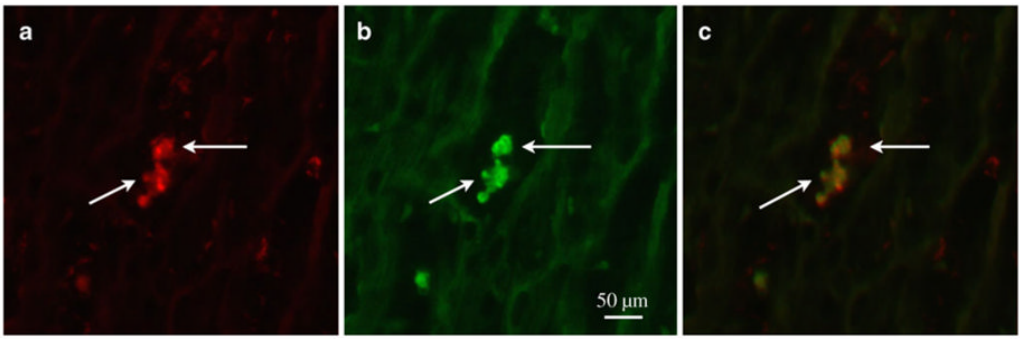

Fig. 6.

Fluorescent microscopic images (×400 magnification) of double immunofluorescence staining on frozen tissue from an allograft on POD 20. **a** A section taining with anti-rat ED1 mAb (for macrophages; *arrows, red*). **b** The same section as *Panel A* staining with anti-rat RT1.A^{a,b,l} mAb (for rat PVG.R8; *arrows, green*). The images shown in *Panels a* and *b* were taken over the same field of view, while *Panel c* is an overlay image of *a* and *b*. These data indicate that recipient immune cells, mainly macrophages, are present at early stages of chronic cardiac rejection. (From Ye et al. [26•]; with permission)

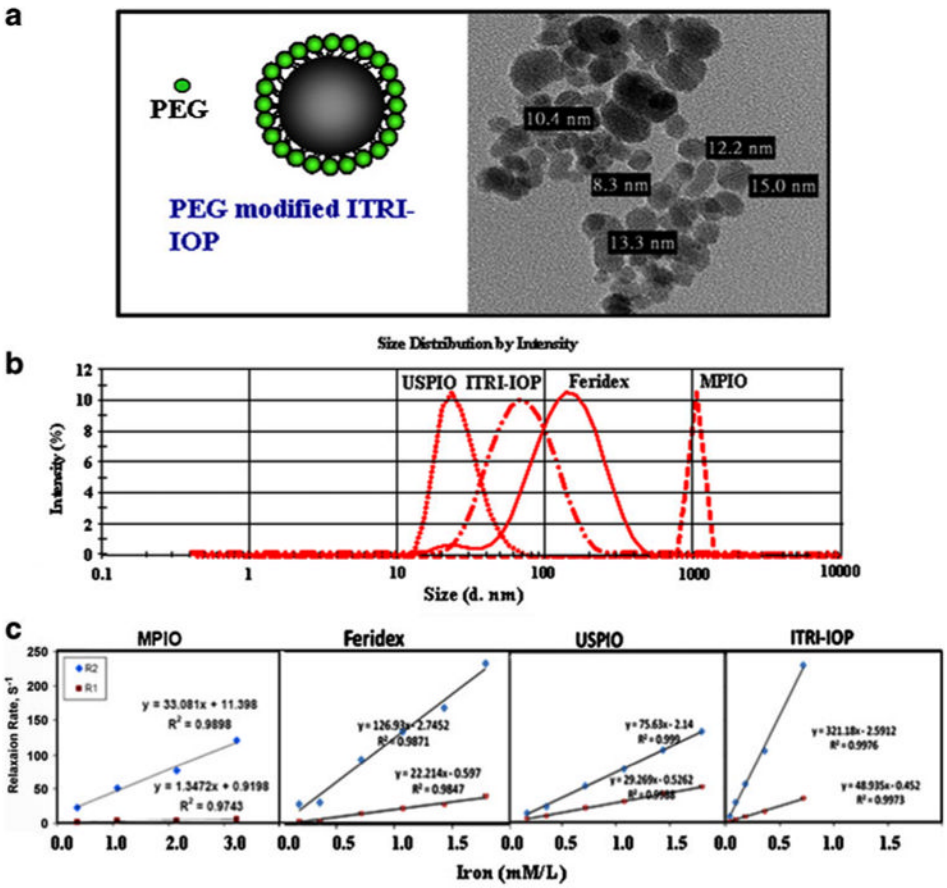

Fig. 7.

Characterization of ITRI-IOP. **a** Schematic drawing of the PEG-coated ITRI-IOP, and the TEM image of the iron core of the ITRI-IOP particles. **b** Dynamic light scattering analysis of the hydrodynamic diameter of iron-oxide particles. Peak intensity is provided for each distribution of particles. **c** r_1 and r_2 relaxivity measurements of four iron-oxide particles diluted in distilled water with iron concentrations between 5–180 μg/mL. The longitudinal and transverse relaxation rates R_1 ($1/T_1$) and R_2 ($1/T_2$) are linearly fitted against iron concentration. The slopes of the linear fitting are the longitudinal and transverse relaxivities, r_1 and r_2, of the particles, respectively. (From Chen et al. [48]; with permission)

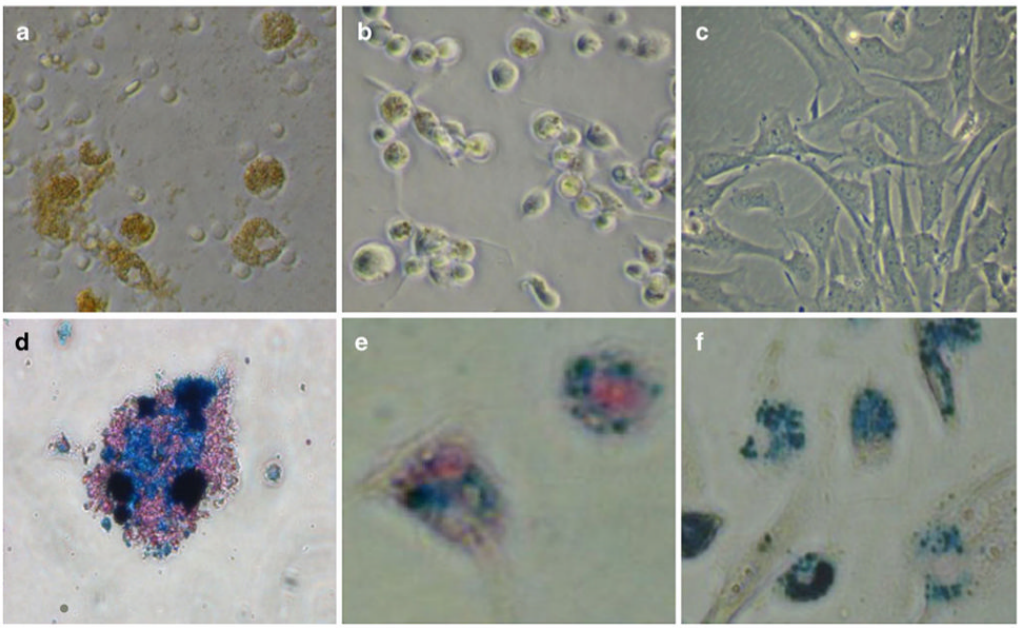

Fig. 8.

Light microscopy of cells labeled with ITRI-IOP. Light microscopy (×200) of **a** macrophages, **b** dendritic cells, and **c** MSCs co-cultured with ITRI-IOP for 24 h, where the *brown* or *light brown* color indicates the incorporation of iron-oxide particles inside cells. Light microscope images (×400) of **d** macrophages, **e** dendritic cells, and **f** MSCs after Prussian blue staining also show the presence of iron in the cell cytoplasm (iron shown as *blue*). (From Chen et al. [48]; with permission)

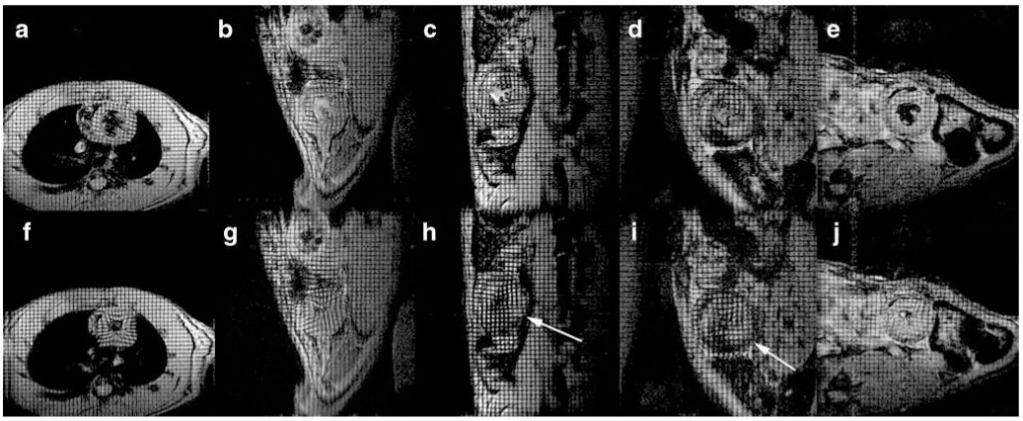

Fig. 9.

MRI tagging. Tagged images for a native heart (**a**, **f**), and the same transplanted hearts shown in Fig. 4 (*see* Wu et al. [22•]). **b, g** is the same isograft shown in Fig. 4a; **c, h** is the allograft shown in Fig. 4c; **d, i** is the allograft shown in Fig. 4d; and **e, j** is the allograft shown in Fig. 4e. *Top panels* **a**–**e**: ED; *lower panels* **f**–**j**: ES. Some areas with compromised wall motion are identified with *arrows*. Some areas with USPIO infiltration can be seen as *dark regions*. Anatomical structures are not labeled for clarity. (From Wu et al. [22•]; with permission)

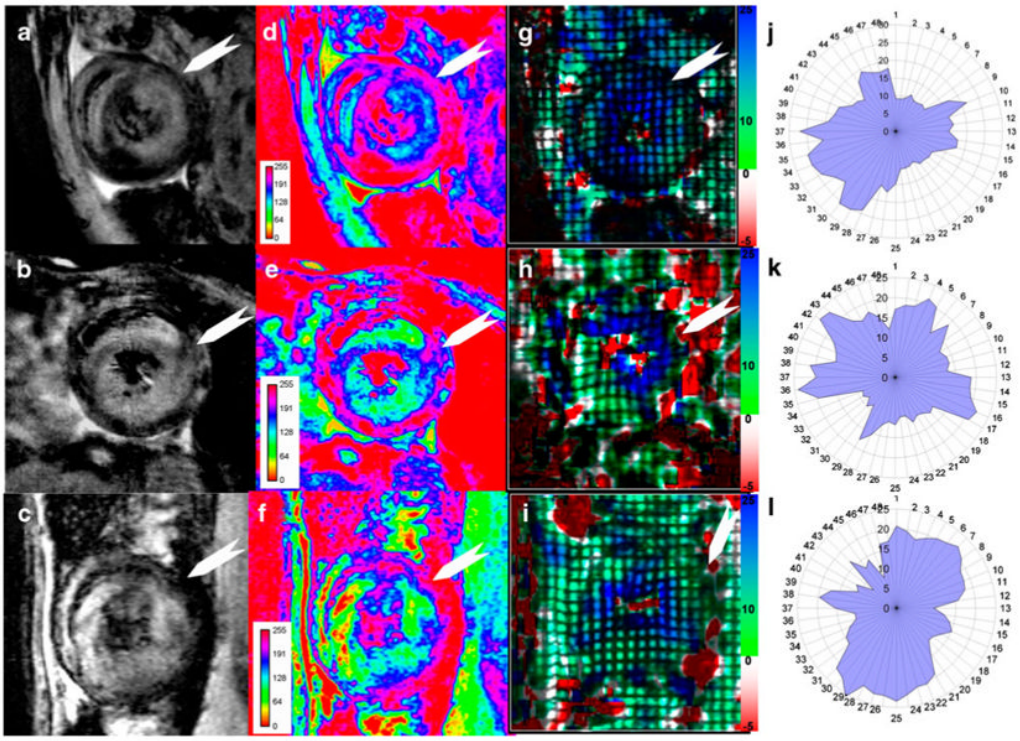

Fig. 10.

Simultaneous tracking of cellular infiltration and function for 3 allografts: **a**–**c**, T_2*-weighted MRI; **d**–**f**, pseudo-coloring of T_2*-weighted images with 8-bit signal-intensity scaling; and **g**–**i**, Ecc strain maps. Absolute or positive values of Ecc are indicated: **j**–**l**, polar plots of |Ecc|. *White arrows* indicate the intercepted point of right ventricle and left ventricle, which is the starting location of probe #1. (From Wu et al. [22•]; with permission)

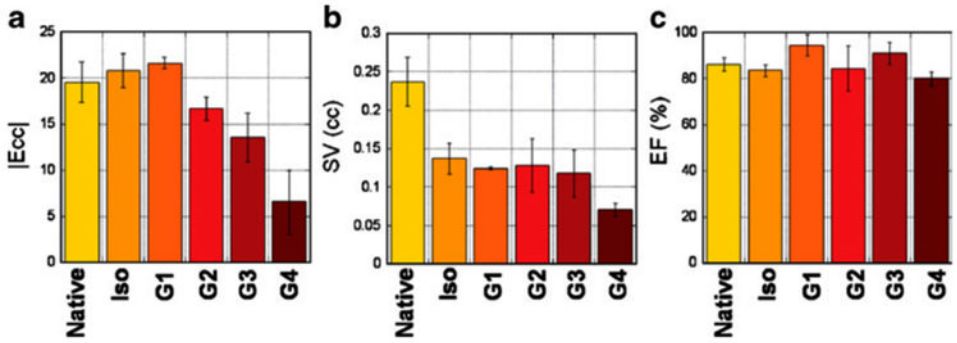

Fig. 11.

Mean Ecc **a**, stroke volume (SV; **b**), and ejection fraction (EF; **c**) for native and transplanted hearts: native, isograft, allograft grade I, grade II, grade III, and grade IV. |Ecc|: absolute or positive values of Ecc strain are used without negative signs. (From Wu et al. [22•]; with permission)

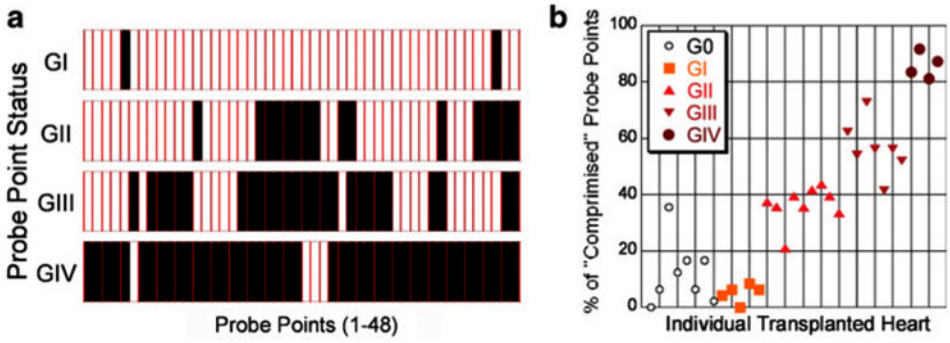

Fig. 12.

Rejection grading by Ecc probe-point values. **a** Numbers of "compromised" probe points for each of grade I (G1), grade II (GII), grade III (GIII), and grade IV (GIV) allografts. Probe-points with "compromised" Ecc strain appear as *solid bars*, whereas probe-points with normal Ecc strain are left *uncolored*. Compromised probe-point is defined as |Ecc| if the particular probe-point is less than one standard deviation from the mean isograft Ecc values. **b** Percent of "compromised" probe-points for individual hearts. (From Wu et al. [22•]; with permission)

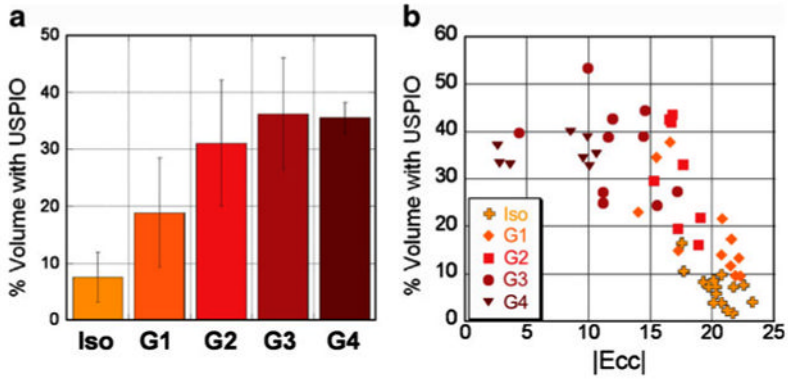

Fig. 13.

Quantitation for USPIO cell infiltration. **a** Percentage of contrast-containing volume from T_2*-weighted images for isografts, grade I, grade II, grade III, and grade IV allografts. **b** Plot percentage of contrast-containing volume against mean Ecc strain for individual heart slices for isografts (*cross*), grade I (*diamond*), grade II (*square*), grade III (*circle*), and grade IV (*triangle*) allografts. Ecc and USPIO volumes for isografts were obtained from different animals is some cases. For each allograft plotted, Ecc and USPIO volumes were obtained from the same animal. (From Wu et al. [22•]; with permission)